AIAA SciTech Forum
7-11 January 2019, San Diego, California
AIAA Scitech 2019 Forum

10.2514/6.2019-0888

Stability and Sensitivity Analysis of a Low-speed Jet in Cross-flow

Marc A. Regan* and Krishnan Mahesh†
Aerospace Engineering & Mechanics, University of Minnesota, Minneapolis, MN 55455, USA

The JICF is studied using direct numerical simulation of the linearized Navier-Stokes equations, as well as their adjoint, at a Reynolds number of 2000, and two jet-to-cross-flow velocity ratios: $R = 2$ with an absolutely unstable upstream shear-layer, and $R = 4$ with a convectively unstable upstream shear-layer. Linear stability analysis of the JICF reveals that the dominant eigenmodes are shear-layer modes whose frequencies match frequencies of the upstream shear-layer observed in simulation and experiment. Asymmetric modes are shown to be more important to the overall dynamics at higher jet-to-cross-flow ratios. Adjoint modes show that the upstream shear-layer is most sensitive to perturbations along the upstream side of the jet nozzle exit. Wavemaker results are shown to be consistent with the transition of the upstream shear-layer from absolute to convective instability.

I. Introduction

Jets in cross-flow (JICF), or transverse jets, are canonical flows where a jet of fluid is injected transverse to an incoming cross-flow. Typically, a flat-plate boundary layer interacts with a wall-normal jet, creating a complex array of inter-related vortical structures. Shear-layer vortices and the Kelvin-Helmholtz instability are typically observed on the upstream side of the jet. The counter-rotating vortex pair (CVP), which dominates the jet cross-section [1, 2], persists far downstream and is a characteristic feature of transverse jets. Additionally, horseshoe vortices are formed near the wall just upstream of the jet exit and wrap around the jet [3, 4]. As the horseshoe vortices travel downstream they begin to tilt upward during 'separation events' [5] caused by the adverse pressure gradient created as the jet entrains fluid from the boundary layer. This process forms wake vortices that extend up in the wall-normal direction through the jet wake [5–9]. Transverse jets are found in many engineering applications, including gas turbine combustors, film cooling, vertical and/or short take-off and landing (V/STOL) aircraft, and controlled fluidic injection (i.e. thrust vectoring). Reviews by Margason [10], Karagozian [11] and Mahesh [12] compile most of the JICF research, both experimental and computational, over the last seven decades. The JICF is characterized by the following parameters: the jet Reynolds number, $Re = \overline{v}_{\text{jet}} D/\nu_{\text{jet}}$, based on the average velocity ($\overline{v}_{\text{jet}}$) at the jet exit, the diameter (D), and the kinematic viscosity of the jet (ν_{jet}); the jet-to-cross-flow velocity ratio (for constant density jets), $R = \overline{v}_{\text{jet}}/u_\infty$, where u_∞ is the cross-flow velocity.

The JICF has been studied using global linear stability in the past [13] using a steady baseflow obtained using selective frequency damping (SFD) [14]. From this point on, linear stability analysis will refer to Tri-Global linear stability analysis unless otherwise specified. It was shown that the shedding frequency for the upstream shear-layer was not far from the non-linear shedding frequency. However, the linear wake mode frequency was far from the non-linear wake frequency. Bagheri et al. [13] suggested that the differences in shedding frequencies could be related to the differences between the SFD solution and the time-averaged solution.

The focus of this paper is to further the understanding of the stability and sensitivity of the JICF using linear stability and adjoint sensitivity analyses around turbulent mean flows. Understanding the dominant flow instability mechanisms, and how they are most sensitive to velocity perturbations will help control of the JICF in engineering applications. Jet-to-cross-flow ratios of 2 and 4 at $Re = 2000$ are chosen, to straddle the upstream shear-layer stability transition observed by Megerian et al. [15]. The upstream shear-layer transition is important since optimizing jet penetration and mixing is shown to be highly dependent on the stability of the shear-layer [15, 16]. The paper is organized as follows. §II describes the numerical methodology. In §III detailed descriptions of the problem and simulation setup are given. §IV discusses the results, followed by a brief summary in §V.

*Graduate Research Assistant, Aerospace Engineering & Mechanics
†Professor, Aerospace Engineering & Mechanics, AIAA Associate Fellow

II. Numerical Methodology

A. Governing equations

Modal linear stability analysis is the study of the dynamic response of a base state (i.e. baseflow) subject to external perturbations (see Theofilis [17] for review). In this paper, the incompressible Navier-Stokes equations are linearized about a base state $\overline{\boldsymbol{u}}_i$ and $\overline{p}$. The base state can be assumed to vary arbitrarily in space ($\overline{\boldsymbol{u}}_i = \overline{\boldsymbol{u}}_i\,(x, y, z)$). If the flow field is decomposed into a base state subject to a small $O(\varepsilon)$ perturbation ($\boldsymbol{u}_i = \overline{\boldsymbol{u}}_i + \varepsilon\tilde{\boldsymbol{u}}_i$, $p = \overline{p} + \varepsilon\tilde{p}$), the linearized Navier-Stokes (LNS) equations may be written as

$$\begin{aligned} \frac{\partial \tilde{\boldsymbol{u}}_i}{\partial t} + \frac{\partial}{\partial x_j}\tilde{\boldsymbol{u}}_i\overline{\boldsymbol{u}}_j + \frac{\partial}{\partial x_j}\overline{\boldsymbol{u}}_i\tilde{\boldsymbol{u}}_j &= -\frac{\partial \tilde{p}}{\partial x_i} + \nu\frac{\partial^2 \tilde{\boldsymbol{u}}_i}{\partial x_j \partial x_j}, \\ \frac{\partial \tilde{\boldsymbol{u}}_i}{\partial x_i} &= 0, \end{aligned} \tag{1}$$

by neglecting the ε^2 terms. For linear stability analysis, we are interested in the behavior of perturbations at asymptotic time of the form

$$\tilde{\boldsymbol{u}}_i\,(x, y, z, t) = \sum_{\omega} \hat{\boldsymbol{u}}_i\,(x, y, z)\, e^{\omega t} + \text{c.c}, \tag{2}$$

where ω and $\hat{\boldsymbol{u}}_i$ can be complex. This reduces the linear system of equations to an eigenvalue problem. We solve the eigenvalue problem using the Implicity Restarted Arnoldi iteration method (IRAM) in conjunction with a time-stepper method.

Adjoint techniques have been shown to be extremely useful in many fluid mechanics applications involving laminar-to-turbulent transition, receptivity, sensitivity, acoustics, and control. By choosing an inner product, an adjoint to the LNS eigenvalue problem may be formed. We choose the energy norm as the inner product, which is defined as:

$$(\boldsymbol{u}, \boldsymbol{v}) = \iiint_V \boldsymbol{u}^{\mathrm{T}}\boldsymbol{v}\;\mathrm{d}x\,\mathrm{d}y\,\mathrm{d}z = \int_\Omega \boldsymbol{u}^{\mathrm{T}}\boldsymbol{v}\;\mathrm{d}\Omega \Longrightarrow \sum_{i=1}^{\mathrm{ncv}} \boldsymbol{u}^{\mathrm{T}}\boldsymbol{v}V_{\mathrm{cv}}, \tag{3}$$

where Ω is the computational volume, $\boldsymbol{u}$ and $\boldsymbol{v}$ are arbitrary vector quantities, ncv is the total number of control volumes, and V_{cv} is the CV volume. By using the generalized Lagrange identity [18], the adjoint to the LNS equations are defined the same as Hill [19]:

$$\begin{aligned} \frac{\partial \tilde{\boldsymbol{u}}_i^\dagger}{\partial t} + \frac{\partial}{\partial x_j}\tilde{\boldsymbol{u}}_i^\dagger\overline{\boldsymbol{u}}_j - \tilde{\boldsymbol{u}}_j^\dagger\frac{\partial}{\partial x_i}\overline{\boldsymbol{u}}_j &= -\frac{\partial \tilde{p}^\dagger}{\partial x_i} - \nu\frac{\partial^2 \tilde{\boldsymbol{u}}_i^\dagger}{\partial x_j \partial x_j}, \\ \frac{\partial \tilde{\boldsymbol{u}}_i^\dagger}{\partial x_i} &= 0, \end{aligned} \tag{4}$$

where $\tilde{\boldsymbol{u}}_i^\dagger$ is the adjoint velocity perturbation and $\tilde{p}^\dagger$ is the adjoint pressure perturbation. Note the opposite sign on the viscous term, which defines that the adjoint equations must be solved backwards in time. Using the same modal decomposition (eq. 2), the linear adjoint equations also reduce to an eigenvalue problem. The adjoint velocity perturbation field, $\tilde{\boldsymbol{u}}_i^\dagger$, highlights points in the flow where a large response to unsteady point forcing will occur [19]. In the present work, adjoint sensitivity analysis is used in conjunction with linear stability analysis to determine flow regions that are most sensitive to point momentum forcing.

B. Algorithm

An unstructured, finite-volume algorithm developed by Mahesh et al. [20] is used to solve the linearized N-S equations (eq. 1) and their adjoint (eq. 4). The spatial discretization emphasizes the simultaneous conservation of discrete first-order quantities (i.e. momentum) and second-order quantities, such as kinetic energy. In other words, $\sum \boldsymbol{u}_i\partial\left(\boldsymbol{u}_i\boldsymbol{u}_j\right)/\partial x_j$ over all control volumes only has contributions from the boundary elements. In this method, Cartesian velocities, u_i, and pressure, p, are stored at the control volume (CV) centroid. Additionally, face-normal velocities, v_n, are stored separately at the centroids of the faces. The algorithm has been validated and used to simulate a variety of complex flows, including: a gas turbine combustor [20], free jet entrainment [21], and transverse jets [22–28], flow over hulls [29, 30] and propellers in crashback [31, 32].

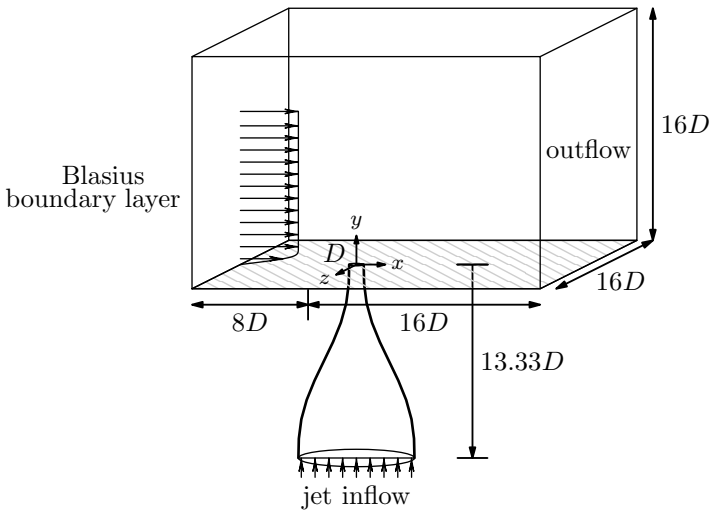

Fig. 1 A schematic of the jet in cross-flow computational domain is shown. The origin is located at the center of the jet exit. A Blasius boundary layer is prescribed as the leftmost inflow condition. Additionally, uniform inflow is prescribed for the jet inflow. The nozzle shape is modeled using a 5th order polynomial that matches the nozzle used in experiments of Megerian et al. [15].

C. Wavemaker

This paper also discusses the receptivity of the JICF to spatially localized feedback. Due to the non-normality of the eigenvalue problem associated with the JICF, adjoint solutions alone cannot describe the whole picture. Therefore, the product for each j-th pair of direct and adjoint global modes is computed as

$$W_j(x,y,z) = \frac{\left\|\hat{\boldsymbol{u}}_i^j\right\|\left\|\hat{\boldsymbol{u}}_i^{j,\dagger}\right\|}{\max\left(\left\|\hat{\boldsymbol{u}}_i^j\right\|\left\|\hat{\boldsymbol{u}}_i^{j,\dagger}\right\|\right)}, \tag{5}$$

which determines the locations that are most sensitive to localized feedback [33] - also called 'wavemaker' regions. Locations where $W \approx 1$ are most sensitive to localized feedback, whereas areas with $W << 1$ are generally not important to the stability of the baseflow.

III. Problem Description

Figure 1 shows the simulation set-up. At the inflow, a laminar Blasius boundary layer profile is prescribed. The boundary layer profile is the same as those used by Iyer and Mahesh [27], and has been shown to match well with experiments at $x/D = -5.5$. The jet nozzle is located at the origin of the computational domain and is included in all simulations. It has been shown by Iyer and Mahesh [27] that the jet nozzle plays a crucial role in setting up the mean flow near the jet exit, thus affecting the stability characteristics of the flow. A fifth-order polynomial is used to model the nozzle shape used in the experiments of Megerian et al. [15]. The jet exit diameter D is 3.81 mm and the average velocity at the jet exit $\overline{v}_{\text{jet}}$ is 8 m s^{-1}. Additional simulation details are outlined in table 1. Simulation cases $R2$ and $R4$ are performed at the same conditions as the experiments of Megerian et al. [15].

The unstructured capabilities of the solver allow the cross-flow domain and jet nozzle to be simulated together. Figure 1 also describes the extent of the computational domain. The domain extends $8D$ upstream of the jet exit to the inflow boundary where the Blasius laminar boundary layer solution is applied. $16D$ downstream of the jet exit is the outflow boundary. In addition, Neumann boundary conditions are applied to the sides located $8D$ from the origin in the span-wise directions. The simulated nozzle extends $13.33D$ below the jet orifice, at which point a uniform inflow is prescribed to achieve the correct velocity at the jet exit. The top of the domain is located $16D$ above the origin and also has a Neumann boundary condition applied.

The computational grid is made up of 138 million elements. There are 86 elements inside of the inflow laminar boundary layer in the y-direction and 320 elements around the jet exit. After making the assumption that downstream

Case	R	$R^* = v_{\text{jet,max}}/u_\infty$	Re	$Re_{\text{cf}} = Du_\infty/\nu_\infty$	θ_{bl}/D
$R2$	2	2.44	2000	1000	0.1215
$R4$	4	4.72	2000	500	0.1718

Table 1 Details are shown for the simulations used to study the stability of the JICF. Jet to cross-flow ratios R of 2 and 4 are studied at a Reynolds number Re of 2000, based on the average velocity $\overline{v}_{\text{jet}}$ at the jet exit and the jet exit diameter D. Also shown is the jet to cross-flow ratio R^*, based on the jet exit peak velocity $v_{\text{jet,max}}$, and the Reynolds number Re_{cf}, based on the cross-flow velocity u_∞. The momentum thickness of the laminar cross-flow boundary layer is described at the jet exit when the jet is turned off.

of the jet exit the boundary layer is turbulent, viscous wall units may be computed (e.g. $\Delta x^+ = \frac{\Delta x u_\tau}{\nu}$). The local wall shear stress is used to calculate the friction velocity ($u_\tau = \sqrt{\tau_w/\rho} = \sqrt{\nu(d\overline{u}/dy|_{y=0})}$). Downstream of the jet exit, the grid maintains spacings of $\Delta x^+ = 2.10$, $\Delta y^+_{\text{min}} = 0.09$, and $\Delta z^+ = 1.45$ for case $R2$ and $\Delta x^+ = 1.09$, $\Delta y^+_{\text{min}} = 0.05$, and $\Delta z^+ = 0.75$ for case $R4$. These grid spacings are finer than the grid used by Muppidi and Mahesh [23] to simulate a turbulent JICF.

Instantaneous isocontours of Q-criterion colored by stream-wise velocity for the turbulent flow-field are shown in figure 2 for case $R2$ (a) and $R4$ (b). The complexity of the turbulent JICF is illustrated by these instantaneous results. Important features include the coherent upstream shear-layer roll up, as well as long string-like wake vortices near the wall. Additionally, downstream shear-layer roll up is seen that interacts with the upstream shear-layer at the collapse of the potential core. Many fine scale turbulent structures are also visible downstream in the jet wake.

The turbulent mean flows that are used as the base states were generated using the 138 million element grid. To generate the mean flows, 54000 and 70000 samples are used for case $R2$ and $R4$, respectively.

IV. Results

This section presents results from the direct and adjoint analyses of cases $R2$ and $R4$. In the following, the behavior in the upstream shear-layer and CVP are discussed. The eigenvalues are non-dimensionalized such that the growth rate is $\text{Re}(\frac{\omega}{2\pi})D/v_{\text{jet,max}}$ and the Strouhal number, St, is $\text{Im}(\frac{\omega}{2\pi})D/v_{\text{jet,max}}$. The adjoint eigenvalues match those from linear stability, and agree well with the upstream shear-layer spectra results from experiments [15] and simulations [27]. The eigenmodes from linear stability analysis are shown using isocontours of the streamwise (x-direction) perturbation velocity, $\text{Re}(\hat{u}) = \pm 0.0003$. Adjoint sensitivity analysis eigenmodes are presented using isocontours of the vertical (y-direction) adjoint perturbation velocity, $\text{Re}(\hat{v}^\dagger) = \pm 0.0001$, which highlight regions most sensitive to vertical point momentum forcing. Eigenmodes are normalized such that $\|\hat{u}\| = \|\hat{v}^\dagger\| = 1$.

A. Upstream shear-layer

The upstream shear-layer linear stability eigenmodes for both case $R2$ (figure 3a) and case $R4$ (figure 4) were discussed in detail by Regan and Mahesh [28]. The main difference between the direct (i.e. linear stability analysis) eigenmodes for each case is that for case $R2$ the mode originates near the jet exit plane, whereas for $R4$ the mode is elevated.

The adjoint eigenmodes (figures 3b and 4b) show that the direct modes are most sensitive to y-direction momentum forcing along the upstream side of the jet nozzle, near the jet exit. Interestingly, for $R2$ the wavemaker region (figure 3c-d) is localized along the upstream side of the nozzle. Conversely, $R4$ (figure 4c-d) is most sensitive to localized feedback along the entire upstream shear-layer.

The wavemaker results are consistent with the notion that the upstream shear-layer region transitions from absolute to convective instability as R changes from 2 to 4. For $R2$, the region most sensitive to localized feedback is dominated by the formation of the upstream shear-layer, which is in direct contrast to case $R4$, which is sensitive to localized feedback along the entire upstream shear-layer. The tonal nature of case $R2$ is due to the fact that the location where the shear-layer roll-up forms is where localized feedback is strongest. Case $R4$ is not only weaker, but includes harmonics due to the wavemaker region extending along the upstream shear-layer.

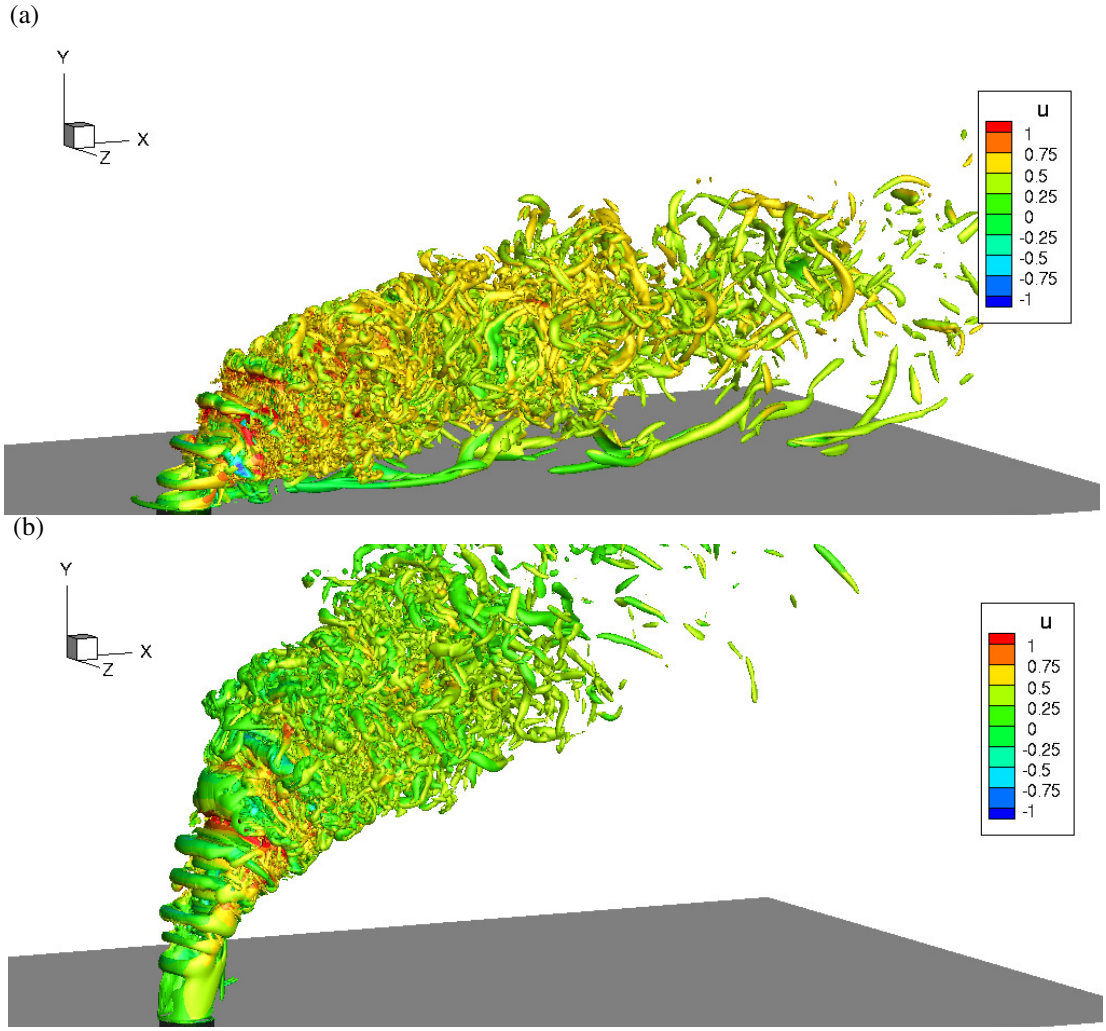

Fig. 2 Isocontours of Q-criterion colored by stream-wise velocity for the instantaneous turbulent flow-field for $R = 2$ (a) and $R = 4$ (b).

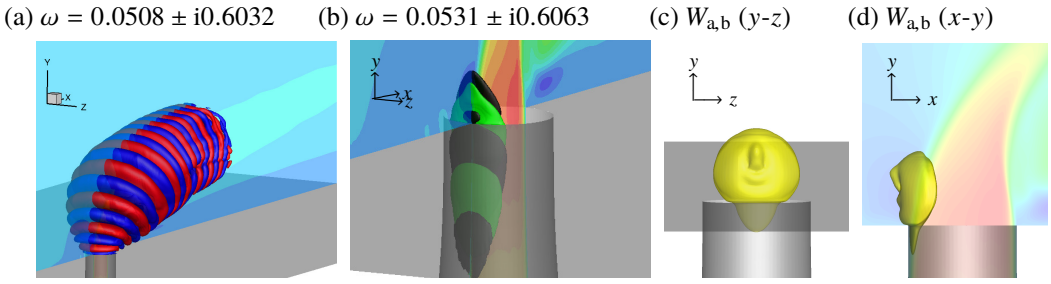

Fig. 3 The $R2$ upstream shear-layer linear stability (a) and adjoint sensitivity analyses (b) eigenmodes along with their associated wavemaker (c-d). Symmetry plane contours show the vertical velocity of the baseflow $\overline{v}$.

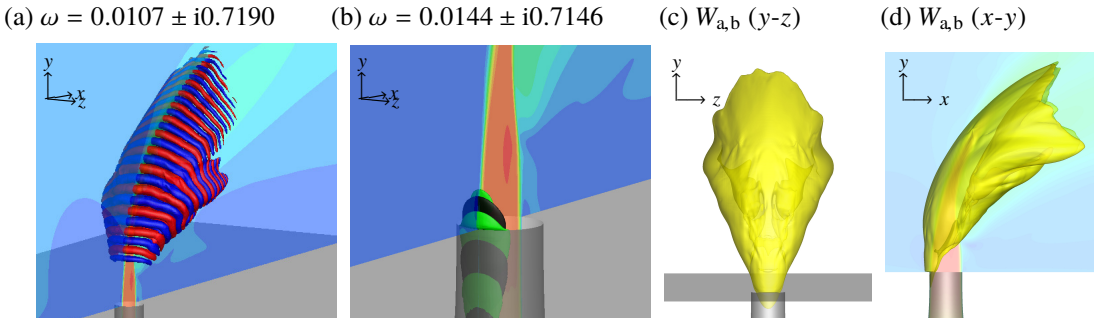

Fig. 4 Similar to figure 3, but for the $R4$ upstream shear-layer.

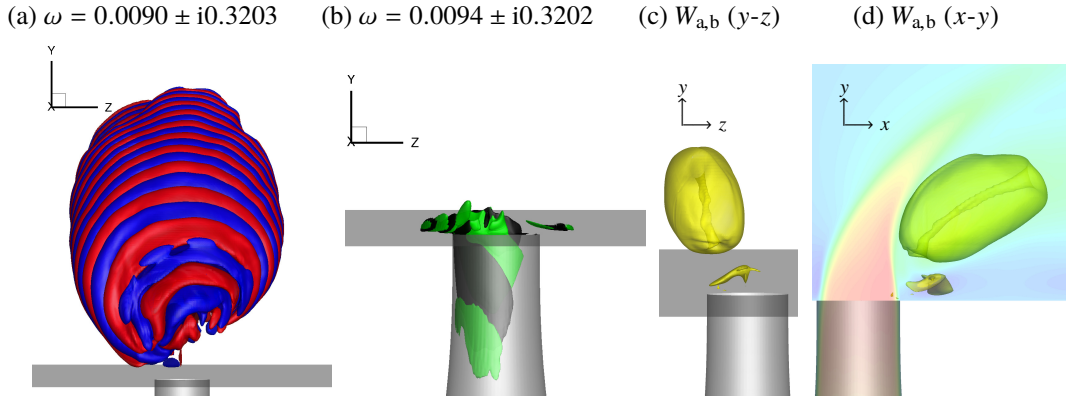

Fig. 5 Similar to figure 3, but for the $R2$ *left-leaning* asymmetric eigenmodes.

B. Asymmetries in the CVP

Smith and Mungal [2] studied the JICF experimentally, and determined that at high jet-to-cross-flow ratios ($R > 10$) asymmetries may form in the time-averaged CVP. Getsinger et al. [34] have also observed asymmetric mean CVP cross-sections in their experiments. They conclude that an absolutely unstable JICF ($R2$) is less likely to exhibit asymmetric mean profiles when compared to the weaker, convectively unstable JICF ($R4$). The reason why the JICF behaves asymmetrically is not fully understood; specifically the reason why there is a preferential direction in certain configurations.

In the present work, we observe significant asymmetries in some eigenmodes. The direct (a) and adjoint (b) eigenmodes in figure 5 for case $R2$, and figure 6 for case $R4$ are *left-leaning* and correspond to a wavemaker region biased towards the left side. Conversely, additional eigenmodes (not shown) are mirrored across the symmetry plane,

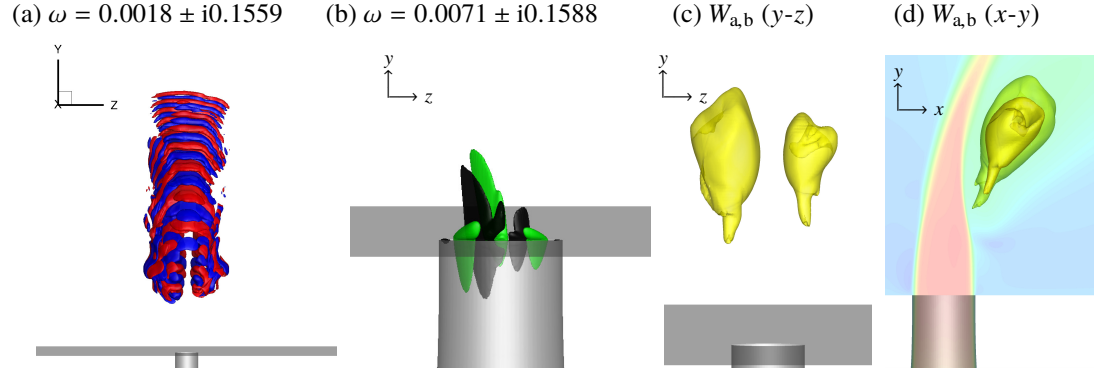

Fig. 6 Similar to figure 3, but for the $R4$ *left-leaning* asymmetric eigenmodes.

and are *right-leaning*. The adjoint eigenmodes (b) are most sensitive to vertical point momentum forcing in a similar way as the upstream shear-layers, but with biases to each side. The wavemakers (c-d) are located along the CVP, directly behind the collapse of the jet potential core. By animating the linear stability analysis eigenmodes (not shown) it is seen that the eigenmodes for both cases rotate with the CVP.

Linear stability analysis results for case $R2$ originate much closer to the jet nozzle exit compared to case $R4$. The adjoint modes provide valuable information regarding the sensitivity of these asymmetric instabilities to y-direction point momentum forcing. Note the spatial and temporal length scales that characterize the regions where asymmetric instabilities are most sensitive. For instance, adjoint sensitivity analysis results for case $R2$ (figure 5b) show much longer length scales in the circumferential direction just below the jet nozzle exit when compared to case $R4$ (figure 6b). This knowledge, in conjunction with the frequency information gathered from animating (not shown) the adjoint sensitivity analysis eigenmodes, provide valuable information regarding the best location and frequencies to excite asymmetries.

Growth rates from the linear stability and adjoint sensitivity analyses are often discussed in terms of their relative strength. We can compute the relative strength of the asymmetric eigenmodes for each case by comparing them to the strength of their respective upstream shear-layer growth rates. The difference $\Delta\omega_{R2}$ between the growth rates of asymmetric eigenmodes and the upstream shear-layer eigenmodes for case $R2$ is in the range $0.042 \leq \Delta\omega_{R2} \leq 0.047$. However, for the $R4$ case, the difference $\Delta\omega_{R4}$ is in the range $0.014 \leq \Delta\omega_{R4} \leq 0.009$. Notice $\Delta\omega_{R2} > \Delta\omega_{R4}$ over their entire ranges, suggesting that asymmetric modes and sensitivity to experimental asymmetries are more significant for $R4$ than $R2$; consistent with experimental results [2, 34].

V. Summary

The sensitivity of the upstream shear-layer mode to vertical point momentum forcing is largest along the upstream side of the jet nozzle for both cases $R2$ and $R4$. Wavemaker results are consistent with the upstream shear-layer stability transition. For case $R2$, the wavemaker is localized near the jet exit, but for case $R4$ the wavemaker is a large region along the upstream shear-layer, and is consistent with the transition from absolute to convective instability.

Asymmetric linear stability and adjoint sensitivity eigenmodes are observed, with *left-leaning* and *right-leaning* direct eigenmodes being most sensitive to vertical forcing on the left- and right-sides, respectively. Additionally, the asymmetric direct modes reside on the CVP. By examining relative growth rates, it is suggested that the asymmetric modes are more relevant to the overall dynamics for case $R4$. Additionally, the spatial length-scales of the adjoint modes provide insight for control strategies.

Acknowledgements

This work was supported by the Air Force Office of Scientific Research (AFOSR) under grant FA9550-15-1-0261. Simulation time was provided by the Texas Advanced Computing Center (TACC) through the Extreme Science and Engineering Discovery Environment (XSEDE) allocation.

References

[1] Kamotani, Y., and Greber, I., "Experiments on a Turbulent Jet in a Cross Flow," *AIAA Journal*, Vol. 10, No. 11, 1972, pp. 1425–1429.

[2] Smith, S. H., and Mungal, M. G., "Mixing, structure and scaling of the jet in crossflow," *Journal of Fluid Mechanics*, Vol. 357, 1998, pp. 83–122.

[3] Krothapalli, A., Lourenco, L., and Buchlin, J. M., "Separated flow upstream of a jet in a crossflow," *AIAA Journal*, Vol. 28, No. 3, 1990, pp. 414–420.

[4] Kelso, R. M., and Smits, A. J., "Horseshoe vortex systems resulting from the interaction between a laminar boundary layer and a transverse jet," *Physics of Fluids*, Vol. 7, 1995, pp. 153–158.

[5] Fric, T. F., and Roshko, A., "Vortical structure in the wake of a transverse jet," *Journal of Fluid Mechanics*, Vol. 279, 1994, pp. 1–47.

[6] Kelso, R. M., Lim, T. T., and Perry, A. E., "An experimental study of round jets in cross-flow," *Journal of Fluid Mechanics*, Vol. 306, 1996, pp. 111–144.

[7] Eiff, O. S., Kawall, J. G., and Keffer, J. F., "Lock-in of vortices in the wake of an elevated round turbulent jet in a crossflow," *Experiments in Fluids*, Vol. 19, 1995, pp. 203–213.

[8] McMahon, H. M., Hester, D. D., and Palfery, J. G., "Vortex shedding from a turbulent jet in a cross-wind," *Journal of Fluid Mechanics*, Vol. 48, 1971, pp. 73–80.

[9] Moussa, Z. M., Trischka, J. W., and Eskinazi, D. S., "The near field in the mixing of a round jet with a cross-stream," *Journal of Fluid Mechanics*, Vol. 80, 1977, pp. 49–80.

[10] Margason, R. J., "Fifty Years of Jet in Cross Flow Research," *Aerospace Research & Development Conference 534*, Winchester, United Kingdom, 1993, pp. 1–41.

[11] Karagozian, A. R., "Transverse jets and their control," *Progress in Energy and Combustion Science*, Vol. 36, No. 5, 2010, pp. 531–553.

[12] Mahesh, K., "The Interaction of Jets with Crossflow," *Annual Review of Fluid Mechanics*, Vol. 45, 2013, pp. 379–407.

[13] Bagheri, S., Schlatter, P., Schmid, P. J., and Henningson, D. S., "Global stability of a jet in crossflow," *Journal of Fluid Mechanics*, Vol. 624, 2009, pp. 33–44.

[14] Akervik, E., Brandt, L., Henningson, D. S., Hœpffner, J., Marxen, O., and Schlatter, P., "Steady solutions of the Navier-Stokes equations by selective frequency damping," *Physics of Fluids*, Vol. 18, No. 6, 2006, p. 068102.

[15] Megerian, S., Davitian, J., Alves, L. S. d. B., and Karagozian, A. R., "Transverse-jet shear-layer instabilities. Part 1. Experimental studies," *Journal of Fluid Mechanics*, Vol. 593, 2007, pp. 93–129.

[16] Sau, R., and Mahesh, K., "Optimization of pulsed jets in crossflow," *Journal of Fluid Mechanics*, Vol. 653, 2010, pp. 365–390.

[17] Theofilis, V., "Global Linear Instability," *Annual Review of Fluid Mechanics*, Vol. 43, 2011, pp. 319–352.

[18] Ince, E. L., *Ordinary Differential Equations*, Dover, 1926.

[19] Hill, D. C., "Adjoint systems and their role in the receptivity problem for boundary layers," *Journal of Fluid Mechanics*, Vol. 292, 1995, pp. 183–204.

[20] Mahesh, K., Constantinescu, G., and Moin, P., "A numerical method for large-eddy simulation in complex geometries," *Journal of Computational Physics*, Vol. 197, 2004, pp. 215–240.

[21] Babu, P. C., and Mahesh, K., "Upstream entrainment in numerical simulations of spatially evolving round jets," *Physics of Fluids*, Vol. 16, No. 10, 2004, pp. 3699–3705.

[22] Muppidi, S., and Mahesh, K., "Study of trajectories of jets in crossflow using direct numerical simulations," *Journal of Fluid Mechanics*, Vol. 530, 2005, pp. 81–100.

[23] Muppidi, S., and Mahesh, K., "Direct numerical simulation of round turbulent jets in crossflow," *Journal of Fluid Mechanics*, Vol. 574, 2007, pp. 59–84.

[24] Muppidi, S., and Mahesh, K., "Direct numerical simulation of passive scalar transport in transverse jets," *Journal of Fluid Mechanics*, Vol. 598, 2008, pp. 335–360.

[25] Sau, R., and Mahesh, K., "Passive scalar mixing in vortex rings," *Journal of Fluid Mechanics*, Vol. 582, 2007, pp. 449–461.

[26] Sau, R., and Mahesh, K., "Dynamics and mixing of vortex rings in crossflow," *Journal of Fluid Mechanics*, Vol. 604, 2008, pp. 389–409.

[27] Iyer, P. S., and Mahesh, K., "A numerical study of shear layer characteristics of low-speed transverse jets," *Journal of Fluid Mechanics*, Vol. 790, 2016, pp. 275–307.

[28] Regan, M. A., and Mahesh, K., "Global linear stability analysis of jets in cross-flow," *Journal of Fluid Mechanics*, Vol. 828, 2017, pp. 812–836.

[29] Chang, P. A., Vargas, A., Jiang, M., Lummer, D., and Mahesh, K., "Fully-resolved LES of weakly separated flows," *20th AIAA Computational Fluid Dynamics Conference*, 2011, pp. 1–23.

[30] Mahesh, K., Kumar, P., Gnanaskandan, A., and Nitzkorski, Z., "LES Applied to Ship Research," *Journal of Ship Research*, Vol. 59, 2015, pp. 238–245.

[31] Verma, A., Jang, H., and Mahesh, K., "The effect of an upstream hull on a propeller in reverse rotation," *Journal of Fluid Mechanics*, Vol. 704, 2012, pp. 61–88.

[32] Jang, H., and Mahesh, K., "Large eddy simulation of flow around a reverse rotating propeller," *Journal of Fluid Mechanics*, Vol. 729, 2013, pp. 151–179.

[33] Giannetti, F., and Luchini, P., "Structural sensitivity of the first instability of the cylinder wake," *Journal of Fluid Mechanics*, Vol. 581, 2007, pp. 167–197.

[34] Getsinger, D. R., Gevorkyan, L., Smith, O. I., and Karagozian, A. R., "Structural and stability characteristics of jets in crossflow," *Journal of Fluid Mechanics*, Vol. 760, 2014, pp. 342–367.